Published in final edited form as:
*Magn Reson Med*. 2012 February ; 67(2): 490–498. doi:10.1002/mrm.23295.

# Prospective Self-Gating for Swallowing Motion: A Feasibility Study in Carotid Artery Wall MRI Using 3D Variable-Flip-Angle TSE

**Zhaoyang Fan**[1,2], **Sven Zuehlsdorff**[2], and **Debiao Li**[1,2,*]

[1]Biomedical Imaging Research Institute, Departments of Biomedical Sciences and Imaging, Cedars-Sinai Medical Center, Los Angeles, CA

[2]Department of Bioengineering, University of California, Los Angeles, CA

[3]Cardiovascular MR R&D, Siemens Healthcare, Chicago, IL

## Abstract

Three-dimensional (3D) black-blood MRI is a promising noninvasive imaging technique for the assessment of atherosclerotic carotid artery disease. However, this technique is inherently susceptible to motion. In particular, swallowing can result in considerable wall motion at the carotid bifurcations, which may induce drastic image degradation or substantial overestimation of wall thickness. Self-gating (SG) techniques have previously been shown to be capable of resolving and compensating for cardiac or respiratory motion during MRI. This work presents an SG-based prospective motion gating scheme that is combined with a 3D variable-flip-angle turbo spin-echo sequence (SPACE) for detecting swallowing motion. SG signal readouts along the superior-inferior direction during each repetition time (TR) period are used to derive the projection profiles of the imaging volume. Based on cross-correlation analysis between the projection profiles and the corresponding reference profiles, swallowing motion can be detected and the motion-contaminated data will subsequently be discarded and reacquired in the next TR. The self-gated SPACE sequence was validated on eight healthy volunteers and two patients and, when compared with the conventional SPACE sequence, proved to be more resistant to swallowing motion and significantly improved image quality as well as the sharpness of carotid artery wall boundaries.

### Keywords

black-blood MRI; carotid artery; swallowing; self-gating

## INTRODUCTION

Three-dimensional (3D) magnetic resonance imaging (MRI) with blood signal attenuation (i.e., black-blood) is rapidly emerging as a promising noninvasive imaging technique for the assessment of atherosclerotic carotid artery disease (1). Distinct advantages of 3D artery wall MRI over its two-dimensional (2D) counterparts include intrinsic high signal-to-noise ratio (SNR) that may be traded for high spatial resolution, large anatomic coverage, and the capability of retrospective visualization of vessel wall from arbitrary directions. All these features can facilitate the identification of atherosclerotic lesions and assessment of the degree of disease as well as the burden of lesions, which is particularly beneficial to

*Corresponding Author: Debiao Li, PhD, Biomedical Imaging Research Institute, Cedars-Sinai Medical Center, Pacific Theatres (PACT) Suite 800, 8700 Beverly Blvd., Los Angeles, CA 90048, Phone: (310) 423-7743, debiaoli@gmail.com.

irregularly geometric carotids (2–6). However, relatively long imaging times associated with high-spatial-resolution 3D MRI render it more susceptible to motion artifacts, such as ghosting or blurring, which interfere with vessel wall visualization. The 3D spatial encoding mechanism of MRI further exacerbates this challenge; typically, even a brief motion event during data acquisition may corrupt the entire 3D dataset instead of just a single 2D slice.

At the carotid artery, swallowing, arterial pulsation, and breathing have been recognized as major sources of motion (7). Awide range of motion amplitude in the transverse plane was demonstrated at the carotid artery wall, spanning from 0.27 mm to 9.2 mm. Recent work showed that the movement of carotids secondary to swallowing is even greater in the superior-inferior (SI) direction than in the left-right (LR) or anterior-posterior (AP) direction of the transverse plane (8). Such considerable wall motion is clearly critical with regard to the normal wall thickness (0.5±0.1 mm) as well as typically used submillimeter spatial resolution (9), thus potentially resulting in drastic image degradation or substantial overestimation of wall thickness (2).

Hence, effective motion gating is highly desirable for 3D MRI of the carotid artery wall. Arterial pulsation-induced motion can be minimized by using electrocardiogram (ECG) gating during the diastolic cardiac phase (10–12). Respiration gating was previously suggested to overcome breathing-related motion (7), but to our knowledge, no research has been conducted for carotid MRI. Several gating approaches have been proposed for swallowing motion. Navigator echoes acquired from the epiglottis can be used to eliminate data acquired during swallowing, but it requires precise placement of navigator bars and may fail when the epiglottis shifts (13). Recently, Chan et al applied a MR-safe coil made from carbon fiber to detect swallowing-related motion at the laryngeal prominence (14). However, additional setup time of up to 15 minutes for the hardware including coil positioning and preamplifier parameters tune-up can markedly prolong scanning.

Self-gating (SG) techniques have been developed to compensate for cardiac and/or respiratory motion primarily in cardiac MRI (15–19). Previous SG methods are typically based on the integral of the imaging volume to detect motion that causes a variation in total signal energy. Recently, investigators proposed to use a one-dimensional (1D) projection of the imaging volume derived from SG signals to effectively resolve the motion that induces translation or distortion of the object profile (20,21). Considering SI-direction shifts and/or distortion of the larynx structure during swallowing, this projection-based SG approach could be applicable to carotid artery wall MRI for swallowing motion detection.

This work presents an SG-based prospective motion gating scheme for swallowing. To demonstrate its effectiveness in carotid artery wall MRI, the scheme was implemented in a 3D variable-flip-angle turbo spin-echo (TSE) sequence, SPACE, which is capable of providing black-blood effects but may suffer from swallowing motion (4). The self-gated SPACE (SG-SPACE) sequence was validated on eight healthy volunteers and two patients and, compared with conventional SPACE, proved to be more resistant to swallowing motion and significantly improved image quality as well as artery wall sharpness.

## MATERIALS AND METHODS

### Projection-based SG

The carotid artery wall has the greatest movement in the SI direction during swallowing (8). The capture of swallowing motion at the carotid would be achieved by investigating its SI movement. Such motion can manifest as profile shifts and/or distortion in the SI projection of the imaging volume. According to the Central Section Theorem, the relationship between the projection of the imaging volume and k-space data is described by

$$\mathcal{F}_{1D}\{\boldsymbol{P}(\boldsymbol{x})\} = \boldsymbol{F}(\boldsymbol{k}_x, \boldsymbol{k}_y = 0, \boldsymbol{k}_z = 0) \quad [1]$$

where x, y, and z represent the SI, LR, and AP directions, respectively, $\mathcal{F}_{1D}\{\boldsymbol{P}(\boldsymbol{x})\}$ is the 1D Fourier transform of the SI projection $\boldsymbol{P}(\boldsymbol{x})$, and $\boldsymbol{F}$ ($\boldsymbol{k}_x$, $\boldsymbol{k}_y$=0, $\boldsymbol{k}_z$=0) denotes the center k-space line along the SI direction. Such a k-space line can therefore serve as an SG signal line to derive $\boldsymbol{P}(\boldsymbol{x})$ through 1D inverse Fourier transform; it can readily be obtained from 3D Fourier transform k-space sampling whereby the readout direction is parallel to the SI direction and the two phase encoding gradients (along LR and AP) are switched off. Motion will then be resolved by matching the projection profile, $|\boldsymbol{P}(\boldsymbol{x})|$, with the reference profile based on the cross-correlation algorithm (20).

## Implementation of SG in SPACE

SPACE is a variant of 3D TSE techniques, with a long echo train composed of variable-flip-angle nonselective refocusing radiofrequency (RF) pulses (22). It features high time efficiency, low power deposition, and a good in-plane black-blood property, and is being advocated as a promising approach to screening artery wall diseases (4,23,24).

To collect SG lines, a commercially available $T_2$-weighted SPACE sequence was modified as follows (Fig. 1): (a) at the first spin-echo where signal readout was originally skipped to avoid rapid signal modulation (25), the phase-encoding and partition-encoding gradient tables were nulled; (b) the last refocusing RF pulse of the pulse train was duplicated immediately after the train to generate one more spin-echo; (c) two SG readouts (denoted as $SG_1$ and $SG_2$) were added, one at the first spin-echo and the other at the last one.

The schematic of the swallowing motion gating procedure employed in SG-SPACE imaging is illustrated in Fig. 2. In each repetition time (TR) period, two SG signal lines are respectively acquired and Fourier transformed to projections. Cross-correlation coefficients (CC) between projection profiles and their corresponding reference profiles are calculated. Bulk motion of the imaging volume during the period of signal acquisition is indicated when either of the two CC values is lower than the corresponding pre-defined threshold, $TH_{CC}$. When motion is detected, the data acquired during the present TR will be discarded and reacquired. All above functionalities are incorporated into the SPACE sequence and online image reconstruction is accomplished using all valid data.

To ensure gating accuracy, $TH_{CC}$ is tailored to individual subjects in a semi-automatic fashion. A $TH_{CC}$ pre-scan mode can be activated through the user interface of the SG-SPACE sequence. The SG signal lines collected during the $6^{th}$ TR are used to generate two reference profiles for $SG_1$ and $SG_2$, respectively. The first 5 TRs are skipped in order for both SG signals to reach a near steady-state level. The data acquisition then continues for additional 10 TRs and a total of 10 CC values are used to calculate $TH_{CC}$ as

$$TH_{CC} = Mean \text{ of CC values} - 3 \times Standard\ Deviation \text{ of CC values} \quad [2]$$

for $SG_1$ and $SG_2$, respectively. With an assumption of the Normal Distribution, the calculated $TH_{CC}$ is lower than 99.85% of the CC values as derived in the absence of motion but expectedly much higher than those acquired during carotid movement. Subjects need to be instructed to breathe normally and abstain from swallowing during this scan. The calculated $TH_{CC}$ values are output to a customer message window.

Following the $TH_{cc}$ pre-scan, SG-SPACE imaging can be conducted using the calculated $TH_{cc}$'s. The reference profiles of $SG_1$ and $SG_2$ are again derived from the 6$^{th}$ TR, with the subject being instructed to breathe normally and abstain from swallowing at the beginning. In addition, due to potential signal drifts (8), reference profiles are purposely allowed to automatically update if "motion" is indicated by $SG_1$ or $SG_2$ for 6 (user-specifiable) consecutive TRs. In this case, the first SG lines collected following the 6 discarded TRs will be used for generating new reference profiles. During the scan, all CC values and accept/reject decision are output to a customer message window so that the scan may be aborted if the "SG-reference update" is thought to be induced by actual bulk motion that causes abrupt drops in CC values.

## Imaging System and Study Population

All scans were performed on a 3T whole-body MR system (MAGNETOM Trio; Siemens AG Healthcare, Erlangen, Germany). The scanner's integrated body coil was used for RF signal transmission. A bilateral four-channel phased array carotid surface coil (Machnet BV, TD Eelde, The Netherlands) was used for signal reception. For simplicity, SG signal was derived from the first channel only. Eight healthy volunteers (3 males and 5 females, age range 18–45 years, mean age 31 years) and two patients with plaques at the carotid bifurcations (2 males, 67 and 75 years, the second patient has random occurrences of shortness of breath) were recruited in the study as approved by our institutional review board and written informed consent was obtained prior to MRI.

## Imaging Protocol

An oblique coronal 3D imaging slab centered at the bilateral carotid bifurcations was prescribed based on a time-of-flight vessel scout. All healthy subjects underwent the following three vessel wall scans using the developed SG-SPACE sequence: a) imaging without swallowing instructions or SG, denoted as "SPACE STL" (STL: still); b) imaging with swallowing instructions but without SG, denoted as "SPACE SWL" (SWL: swallow); c) imaging with both swallowing instructions and SG (following a $TH_{cc}$ pre-scan), denoted as "SPACE SWL+SG". The latter two scans were performed in a randomized order following the "SPACE STL" scan. On the other hand, the two patients underwent only two scans, SPACE without and with SG, in a random order. ECG-triggering was used to minimize arterial pulsatile-related wall motion (12). Healthy subjects were instructed to hold their head and neck still and breathe normally to ensure that swallowing would be the major source of non-pulsatile motion. K-space raw data including SG signals from the "SPACE SWL+SG" scan on healthy subjects or SPACE scan with SG on patients were saved for retrospective analysis.

The relevant imaging parameters of SPACE imaging included: echo time (TE)/TR 141 msec/3 R-R intervals, trigger delay 450–650 msec, echo train length 74 (including 2 SG echoes), 3 shots per partition, two contiguous partitions interleaved in each TR, coronal acquisition with readouts in the SI direction, FOV 140×140 mm$^2$, matrix 198×192 (interpolated to 396×384), 40 slices of 0.72-mm thickness (interpolated to 80 slices of 0.36-mm thickness), voxel size 0.35×0.36×0.36 mm$^3$, linear view ordering in both phase-encoding and partition-encoding directions, 2 short-term signal averages, generalized autocalibrating partially parallel acquisitions [GRAPPA] with an acceleration factor of 2 along the phase-encoding direction, receiver bandwidth 449 Hz/pixel, spectral-selective fat saturation, acquisition time 120 TRs per scan in the absence of motion.

In the "SPACE SWL" and "SPACE SWL+SG" scans, healthy subjects were instructed over the intercom to swallow twice at five non-equidistant (to avoid ghosting artifacts) preset stages, namely the 30$^{th}$, 50$^{th}$, 60$^{th}$, 70$^{th}$, and 90$^{th}$ TR of the scan ideally free of motion.

These stages were indicated to the operator by customer messages. A break of 2 minutes was given to subjects between the two scans.

## Data Analysis

**Healthy Subject—**Swallowing-induced motion present in the "SPACE SWL+SG" scan was retrospectively analyzed by computing SI projections and CC values from k-space raw data using a custom MATLAB program (version 7.0; The MathWorks, Natick, MA, USA). The necessities of the "SG-reference update" and "dual SG" were respectively explored as follows. The number of motion-contaminated TRs (i.e. CC < $TH_{cc}$) were calculated a) using the SG line from the $6^{th}$ TR only as the reference profile as well as b) employing the "SG-reference update", and a paired two-tailed Wilcoxon signed rank test (SPSS v.16.0; SPSS Inc, Chicago, IL, USA) was used to evaluate the difference between the two cases. With the "SG-reference update" activated, the numbers of TRs with motion detected respectively by $SG_1$ and $SG_2$ were then calculated.

Randomized 3D images of all subjects from three SG-SPACE scans were blindly reviewed by two readers in consensus on a workstation (Leonardo; Siemens Healthcare, Erlangen, Germany). After 2-mm-thick multi-planar reformation (MPR) from the transverse view, each carotid artery was graded on the basis of vessel wall delineation continuity and boundary blurring, particularly at the carotid bifurcation and its vicinity. A 5-point scale was used with half-point scores allowed: 0, very poor wall delineation or unusable images; 1, incomplete wall delineation and severe boundary blurring; 2, moderate wall delineation with appreciable boundary blurring at some locations; 3, good wall delineation with minor boundary blurring at some locations; 4, excellent wall delineation with little or no boundary blurring. Residual flow artifacts due to incomplete blood-suppressing effects were not taken into account during image scoring.

Moreover, vessel wall sharpness at the inner and outer boundaries of healthy subjects was quantified based on a previously used method (26). From each 3D image set, three 2D cross-sectional images of 0.36-mm thickness at spacing of approximately 1 cm (internal carotid artery, carotid bifurcation, and common carotid artery, respectively) were reconstructed with MPR for each carotid artery. Using a custom MATLAB program, individual 2D images were magnified four times through bilinear interpolation, and signal intensity profiles were generated along user-selected lines that perpendicularly traversed the vessel wall at 3 dispersed locations. On each side of the signal intensity profile, the 20% and 80% points between the maximal wall signal intensity and background (surrounding tissues at outer wall boundary or the lumen at inner wall boundary) signal intensity were identified. The distance in millimeters between the two points was then determined and subsequently averaged among the 3 locations of each 2D section. Sharpness was calculated as the reciprocal of the averaged distance for the inner or outer boundaries, respectively. Due to the potential variability in the extent of motion and signal intensities of surrounding tissues, sharpness was not averaged between inner and outer boundaries or among the three longitudinally located 2D sections. The locations of 2D cross-sectional images and user-selected lines for obtaining signal intensity profiles were matched among the three SPACE image sets in each subject.

The image scores and sharpness measurements obtained from the "SPACE SWL+SG" scan were compared with those obtained from the "SPACE STL" and "SPACE SWL" scans using SPSS (v.16.0; SPSS Inc, Chicago, IL, USA). A paired two-tailed Wilcoxon signed rank test was used for the analysis of ordinal image scores and a paired two-tailed Student's *t* test used for the assessment of arterywall sharpness. In all statistical analyses, significance level was defined at $p < 0.05$. Data was presented as mean ± standard deviation.

**Patients—**The number of discarded TRs during SG-SPACE imaging was retrospectively derived. The 3D images from SPACE without and with SG were reviewed on a workstation with focus on the plaques at the carotid bifurcation.

# RESULTS

## Healthy Subjects

Seven healthy subjects (i.e. 14 carotids) were included in qualitative and quantitative analyses. The excluded healthy subject showed severe motion artifacts and low vessel wall SNR in all three SPACE scans (quality score ≤ 1), presumably due to noncooperation or discomfort. $TH_{cc}$ pre-scans provided higher thresholds for $SG_1$ (0.998 ± 0.002) than for $SG_2$ (0.94 ± 0.05). With those pre-defined thresholds, instructed swallowing events were always detected, as clearly indicated by output custom messages. Representative time courses of projection profiles and CC values from $SG_1$ and $SG_2$ were retrospectively derived, as shown in Fig. 3 a–d. The CC-value time courses reveal an intra- and inter-subject variability in the extent and frequency of swallowing, reflecting the fact that swallowing upon instruction was perhaps not a consistent motion event. The projection profile when swallowing motion was present deviated substantially in shape and magnitude from the reference projection profile (Fig. 3 e), thereby leading to $CC < TH_{cc}$.

The real-time “SG-reference update” occurred once or twice in 3 of 7 subjects during the “SPACE SWL+SG” scan (indicated by the numbers above the left bars of each subject in Fig. 4). The left and right bars of each subject in Fig. 4 represent the number of TRs considered to have motion present if the real-time “SG-reference update” was performed and not performed, respectively. Omission of this procedure appeared to give rise to a drastic increase in scan times (The number of valid TRs: 120; the number of discarded TRs in all 7 subjects: 48 ± 45 vs. 27 ± 22, $p = 0.109$), especially in some subjects (subject #1, #3, and #6 in Fig. 4), presumably because the data acquisition could be stalled with an “outdated” reference profile. Of note, all right bars were derived from the data acquired in the context of imaging with the real-time “SG-reference update” and would otherwise be much higher.

In addition, as suggested in Fig. 3 and 4, motion was not always detected simultaneously by both $SG_1$ and $SG_2$. The dual gates approach appeared nontrivial in some cases where little overlap of motion detection between $SG_1$ and $SG_2$ existed (the middle portion of the left bars of each subject in Fig. 4).

In general, swallowing motion resulted in severe blurring of artery wall boundaries, impaired wall continuity, and reduced wall-tissue contrast on non-gated images, which were dramatically improved by means of SG. Representative images at transversal and longitudinal views are shown in Fig. 5 and 6, respectively. The immunity of SG to motion was qualitatively validated by image quality scores (Table 1). Specifically, an acceptable image quality score was obtained in the “SPACE SWL+SG” scan. The score was significantly higher than that ($p = 0.001$) obtained in the “SPACE SWL” scan, although it was significantly lower than that ($p = 0.002$) obtained in the “SPACE STL” scan. Moreover, the sharpness of wall boundaries was preserved by exploiting SG with the “SPACE STL” scan as a reference (outer boundary: 1.95 ± 0.27 vs. 2.02 ± 0.28, $p = 0.232$; inner boundary: 1.78 ± 0.24 vs. 1.86 ± 0.24, $p = 0.121$), but it significantly deteriorated when swallowing was not gated (outer boundary: 1.95 ± 0.27 vs. 1.73 ± 0.37, $p = 0.003$; inner boundary: 1.78 ± 0.24 vs. 1.56 ± 0.36, $p < 0.001$).

### Patients

The discarded TRs were 11 and 17, respectively, in the two patients during SG-SPACE imaging. The $TH_{cc}$ used for $SG_1/SG_2$ were 0.993/0.96 and 0.994/0.97, respectively. Regular SPACE imaging provided blurred images in both patients. In the patient who has random occurrences of shortness of breath, the SPACE images were essentially non-diagnostic (Fig. 7a). In contrast, the SG-SPACE technique dramatically improved the image quality and the lesions were much better depicted. Notice in Fig. 7b that the calcification and thin fibrous cap (arrowhead) at the plaque shoulder region is clearly identified, indicating a vulnerable plaque in the patient.

## DISCUSSION

Despite noticeable advantages in vessel wall imaging, 3D black-blood MRI is inherently susceptible to motion coinciding with the data acquisition. This would be more critical when high-spatial-resolution imaging is performed since the magnitude of movement might exceed the pixel size and the associated low SNR could be further reduced by motion-induced apparent image noise. Swallowing can result in the greatest motion at the carotid bifurcation and its vicinity when compared to arterial pulsation and respiration (7). Thus, swallowing motion gating is beneficial for 3D carotid artery wall MRI.

To our knowledge, this is the first report to investigate the feasibility of applying the SG technique to carotid artery wall MRI. In this work, swallowing on healthy subjects was shown to induce severe overall image degradation, obscure wall boundary, and even cause signal voids in the artery wall with SPACE imaging. The proposed SG approach significantly mitigated the above problems. Further, in comparison with regular SPACE imaging (no SG or swallowing instructions), the SG-SPACE sequence provided slightly impaired yet acceptable image quality and statistically comparable wall boundary sharpness in the presence of swallowing events. Considerable improvement with the SG approach has also been observed in two patients with carotid artery disease, although the detected motion was probably not only secondary to swallowing.

Several technical aspects proposed in this work are considered to impact the above performance. First, image projections are derived from SG signals and exploited to detect swallowing motion. This proved to be sufficiently sensitive to swallowing motion. According to literature (20), cross-correlation analysis is an effective technique to determine motion from the SG projections. CC thresholds are semi-automatically determined through a pre-scan in this work. This makes it possible to tailor the SG technique to individual subjects. An empirical CC threshold derived from a pilot study may not work well for a large population, especially a patient group. The extra time required for the pre-scan is a drawback, but it only adds approximately 30 seconds.

Second, the dual-gate configuration is aimed to create a narrow time window for reliably detecting motion. Intuitively, a single SG line acquired immediately before the readout in each TR may not be adequate to detect motion if the readout duration is relatively long (i.e. approximately 300 msec in SPACE). In this work, the two SG lines appeared to complement each other in detecting motion events. Despite the inherent signal normalization feature in the cross-correlation algorithm, motion-free projections derived from adjacent $SG_1$ and $SG_2$ readouts can still be mutually distorted because of the long-time signal decay of various tissues at heterogeneous transverse relaxation rates. As a result, two separate reference projection profiles are required. It is also noteworthy that two distinct SG thresholds were determined for each subject, with the $SG_2$ threshold substantially lower. This is likely due to the impact of SNR on CC computation (27).

Third, the real-time update of reference projection has been employed. Our previous experience has shown that a fixed reference projection along with a fixed CC threshold may cause data acquisition to stall at some point if the rejection logic is always true. This can be caused by either the bulk motion of the neck or involuntary signal drift (8). In this work, real-time update of the reference projection occurred in three of seven volunteers in which case considerable reduction in scan times resulted, suggesting the necessity of this procedure. Of course, if bulk motion occurs, the update of the reference projection may introduce more image artifacts, a technical limitation. It is therefore advised that scans should be aborted if abrupt drops in CC values are observed at the custom message window.

Last, an intriguing feature of the proposed technique is prospective motion gating. Most of previously proposed SG techniques require retrospective manipulation to eliminate motion corrupted data (15–18,20). By taking advantage of the long idle period following signal acquisition during each TR period, processing of SG signals can be performed and a real-time feedback of accept/reject decision is delivered to the imaging console prior to data acquisition in the next TR. The original online reconstruction program can still work without any adaption.

However, it should be pointed out that the image quality obtained from the “SPACE SWL +SG” scan is slightly inferior to that obtained from the “SPACE STIL” scan and the difference was statistically significant. This could potentially be attributed to heart-rate variability-induced artifacts that commonly follows swallowing (14); variable $T_1$ recovery between echo trains would introduce signal modulation and thus image blurring. Discarding data collected several TRs right before and after the detection of swallowing may help reduce image degradation.

Applications of the proposed SG method may not be limited to the materials presented here. Besides swallowing motion gating, it may also be applied to detect breathing-induced motion. Boussel et al. has reported that respiration can induce motion with amplitude of 1.56 mm that is large enough to compromise the apparent spatial resolution in 3D MRI and degrade vessel wall delineation (7). This could be particularly problematic in patients with respiratory distress who may inflate their lungs in a greater extent and thus induce more movements of the carotids. Considering the different movement extent between swallowing and breathing, the effectiveness of the present method for this application merits an investigation. Moreover, the SG scheme can readily be incorporated into other 2D or 3D vessel wall imaging sequences after minor modification. Not necessarily following the way used in this work, SG signals may be collected through a separate gradient-echo-based preparative module before and after the image data acquisition section of each TR (20).

There are some limitations in this work. Instructed swallowing at five preset stages is still not a well-controlled motion event. Some patients could not have cooperated well and perhaps swallowed once or more than twice. This issue along with different swallowing extent and duration per swallowing among subjects has likely contributed to the large variability in the number of discarded TRs, as shown in Figure 4. In addition, the extent and number of swallowing events during the “SPACE SWL” and “SPACE SWL+SG” scans in the same subject could be non-identical. Such inconsistency would potentially make the comparison of images between these two scans somewhat unfair. However, this issue is likely more unfavorable to “SPACE SWL+SG” scans because more non-instructed motion events could be encountered in a prolonged scan time. Another limitation is that only two patients participated in this feasibility study. Given that carotid atherosclerosis is a common disease in elderly people, complex motion patterns due to respiratory distress or other geriatric illness may present challenges to the technique. This clearly underscores the need for larger-scale clinical studies.

In conclusion, a prospective SG scheme has been developed to detect swallowing motion during carotid artery wall MRI. This preliminary study with SG-SPACE MRI has demonstrated its effectiveness in reducing swallowing-related motion artifacts. This may greatly enhance the clinical value of 3D black-blood MRI in the assessment of carotid atherosclerosis.

## Acknowledgments

Grant sponsor: National Institutes of Health (NIH): 1R01HL096119

## References

1. Fayad ZA, Fuster V. Clinical imaging of the high-risk or vulnerable atherosclerotic plaque. Circulation research. 2001; 89:305–316. [PubMed: 11509446]
2. Balu N, Chu B, Hatsukami TS, Yuan C, Yarnykh VL. Comparison between 2D and 3D high-resolution black-blood techniques for carotid artery wall imaging in clinically significant atherosclerosis. J Magn Reson Imaging. 2008; 27:918–924. [PubMed: 18383253]
3. Crowe LA, Gatehouse P, Yang GZ, Mohiaddin RH, Varghese A, Charrier C, Keegan J, Firmin DN. Volume-selective 3D turbo spin echo imaging for vascular wall imaging and distensibility measurement. J Magn Reson Imaging. 2003; 17:572–580. [PubMed: 12720267]
4. Fan Z, Zhang Z, Chung YC, Weale P, Zuehlsdorff S, Carr J, Li D. Carotid arterial wall MRI at 3T using 3D variable-flip-angle turbo spin-echo (TSE) with flow-sensitive dephasing (FSD). J Magn Reson Imaging. 2010; 31:645–654. [PubMed: 20187208]
5. Luk-Pat GT, Gold GE, Olcott EW, Hu BS, Nishimura DG. High-resolution three-dimensional in vivo imaging of atherosclerotic plaque. Magn Reson Med. 1999; 42:762–771. [PubMed: 10502766]
6. Koktzoglou I, Li D. Submillimeter isotropic resolution carotid wall MRI with swallowing compensation: imaging results and semiautomated wall morphometry. J Magn Reson Imaging. 2007; 25:815–823. [PubMed: 17345637]
7. Boussel L, Herigault G, de la Vega A, Nonent M, Douek PC, Serfaty JM. Swallowing, arterial pulsation, and breathing induce motion artifacts in carotid artery MRI. J Magn Reson Imaging. 2006; 23:413–415. [PubMed: 16463340]
8. Chan, CF.; Gatehouse, PD.; Pennell, DJ.; Firmin, DN. The potential problems associated with carotid motion in carotid artery imaging. Proceedings of the 17th Annual Meeting of ISMRM; Honolulu, Hawai'i, USA. 2009. p. 1829
9. Pauletto P, Palatini P, Da Ros S, Pagliara V, Santipolo N, Baccillieri S, Casiglia E, Mormino P, Pessina AC. Factors underlying the increase in carotid intima-media thickness in borderline hypertensives. Arteriosclerosis, thrombosis, and vascular biology. 1999; 19:1231–1237.
10. Saloner D, Selby K, Anderson CM. MRA studies of arterial stenosis: improvements by diastolic acquisition. Magn Reson Med. 1994; 31:196–203. [PubMed: 8133755]
11. Al-Kwifi O, Kim JK, Stainsby J, Huang Y, Sussman MS, Farb RI, Wright GA. Pulsatile motion effects on 3D magnetic resonance angiography: implications for evaluating carotid artery stenoses. Magn Reson Med. 2004; 52:605–611. [PubMed: 15334581]
12. Sarkar, R.; Moody, AR.; Leung, G. Effect of cardiac gating in high-resolution MRI of the carotid vessel wall. Proceedings of the 17th Annual Meeting of ISMRM; Honolulu, Hawai'i, USA. 2009. p. 1825
13. Crowe LA, Keegan J, Gatehouse PD, Mohiaddin RH, Varghese A, Symmonds K, Cannell TM, Yang GZ, Firmin DN. 3D volume-selective turbo spin echo for carotid artery wall imaging with navigator detection of swallowing. J Magn Reson Imaging. 2005; 22:583–588. [PubMed: 16161101]
14. Chan CF, Gatehouse PD, Hughes R, Roughton M, Pennell DJ, Firmin DN. Novel technique used to detect swallowing in volume-selective turbo spin-echo (TSE) for carotid artery wall imaging. J Magn Reson Imaging. 2009; 29:211–216. [PubMed: 19097078]
15. Larson AC, White RD, Laub G, McVeigh ER, Li D, Simonetti OP. Self-gated cardiac cine MRI. Magn Reson Med. 2004; 51:93–102. [PubMed: 14705049]

16. Spraggins TA. Wireless retrospective gating: application to cine cardiac imaging. Magnetic resonance imaging. 1990; 8:675–681. [PubMed: 2266792]
17. White RD, Paschal CB, Clampitt ME, Spraggins TA, Lenz GW. Electrocardiograph-independent, “wireless” cardiovascular cine MR imaging. J Magn Reson Imaging. 1991; 1:347–355. [PubMed: 1802148]
18. Hiba B, Richard N, Janier M, Croisille P. Cardiac and respiratory double self-gated cine MRI in the mouse at 7 T. Magn Reson Med. 2006; 55:506–513. [PubMed: 16463350]
19. Buehrer M, Curcic J, Boesiger P, Kozerke S. Prospective self-gating for simultaneous compensation of cardiac and respiratory motion. Magn Reson Med. 2008; 60:683–690. [PubMed: 18727084]
20. Lai P, Larson AC, Bi X, Jerecic R, Li D. A dual-projection respiratory self-gating technique for whole-heart coronary MRA. J Magn Reson Imaging. 2008; 28:612–620. [PubMed: 18777542]
21. Stehning C, Bornert P, Nehrke K, Eggers H, Stuber M. Free-breathing whole-heart coronary MRA with 3D radial SSFP and self-navigated image reconstruction. Magn Reson Med. 2005; 54:476–480. [PubMed: 16032682]
22. Mugler, JP., III; Wald, LL.; Brookeman, JR. T2-weighted 3D spin-echo train imaging of the brain at 3 Tesla: reduced power deposition using low flip-angle refocusing RF pulses. Proceedings of the 9th Annual Meeting of ISMRM; Glasgow, Scotland. 2001. p. 438
23. Zhang Z, Fan Z, Carroll TJ, Chung Y, Weale P, Jerecic R, Li D. Three-dimensional T2-weighted MRI of the human femoral arterial vessel wall at 3. 0 Tesla. Investigative radiology. 2009; 44:619–626. [PubMed: 19692844]
24. Mihai G, Chung YC, Merchant A, Simonetti OP, Rajagopalan S. T1-weighted-SPACE dark blood whole body magnetic resonance angiography (DB-WBMRA): initial experience. J Magn Reson Imaging. 2010; 31:502–509. [PubMed: 20099365]
25. Park J, Mugler JP 3rd, Horger W, Kiefer B. Optimized T1-weighted contrast for single-slab 3D turbo spin-echo imaging with long echo trains: application to whole-brain imaging. Magn Reson Med. 2007; 58:982–992. [PubMed: 17969106]
26. Li D, Carr JC, Shea SM, Zheng J, Deshpande VS, Wielopolski PA, Finn JP. Coronary arteries: magnetization-prepared contrast-enhanced three-dimensional volume-targeted breath-hold MR angiography. Radiology. 2001; 219:270–277. [PubMed: 11274569]
27. Parrish TB, Gitelman DR, LaBar KS, Mesulam MM. Impact of signal-to-noise on functional MRI. Magn Reson Med. 2000; 44:925–932. [PubMed: 11108630]

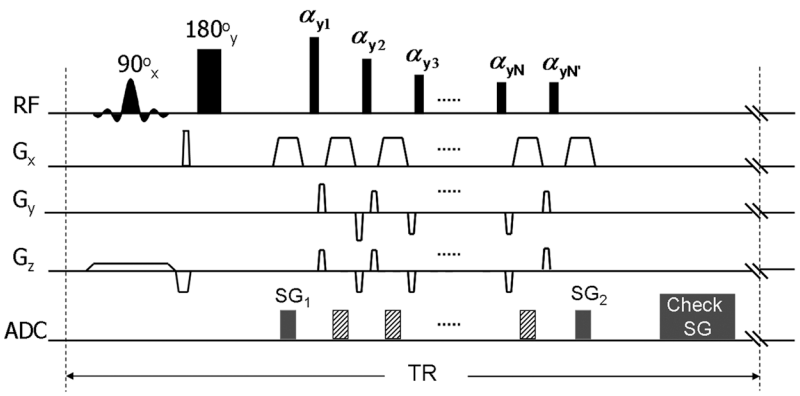


**Fig. 1.**

The sequence diagram of the $T_2$-weighted self-gated SPACE (SG-SPACE) sequence. The conventional $T_2$-weighted SPACE acquisition employs a slab-selective excitation RFpulse ($90°_x$) and a spatially nonselective refocusing ($180°_y$) pulse followed by a series of variable-flip-angle nonselective refocusing pulses ($\alpha_{y1}$, $\alpha_{y2}$, $\alpha_{y3}$,…, $\alpha_{yN}$). The SG-SPACE sequence requires the following modifications: i) at the first spin-echo, the phase-encoding ($G_y$) and partition-encoding ($G_z$) gradient tables were nulled; ii) the last refocusing RF pulse of the pulse train was duplicated ($\alpha_{yN'}$) immediately after the train to generate one more spin-echo; iii) two SG readouts (denoted as $SG_1$ and $SG_2$) were added, one at the first spin-echo and the other at the last one. The accept/reject decision is made based on the analysis of SG signals before the data acquisition in the next TR.

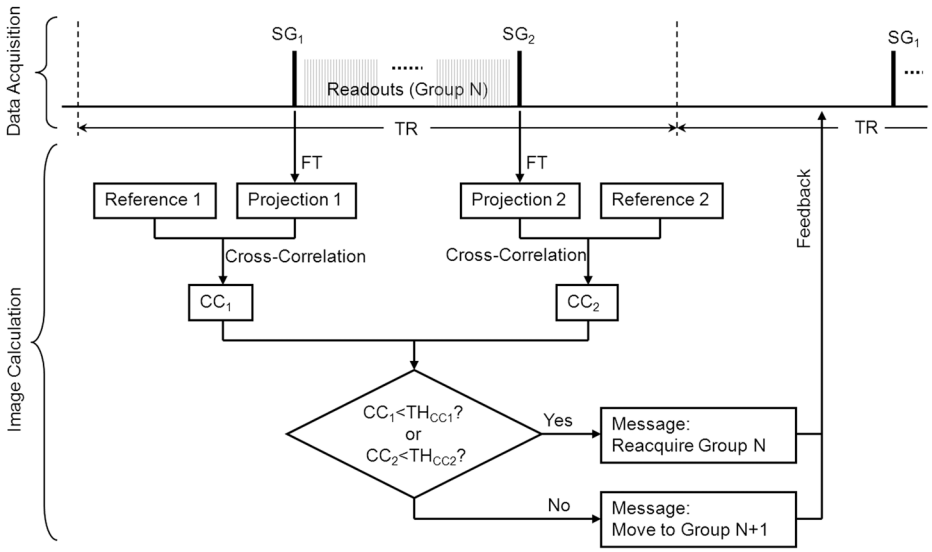


**Fig. 2.**

The schematic of the SG procedures employed in the SG-SPACE sequence. In each TR period, two SG signal lines ($SG_1$ and $SG_2$) are acquired in the data acquisition module and transferred to the image calculation module to undergo a series of processing. They are first Fourier transformed (FT) to projections. Cross-correlation coefficients (CC) between projection profiles and their corresponding reference profiles are then calculated. When either of the two CC values is lower than the corresponding pre-defined threshold, $TH_{CC}$, a feedback message of "reacquiring the present data group" will be delivered back to the data acquisition module. Otherwise, a feedback message of "moving to the next data group" will be delivered.

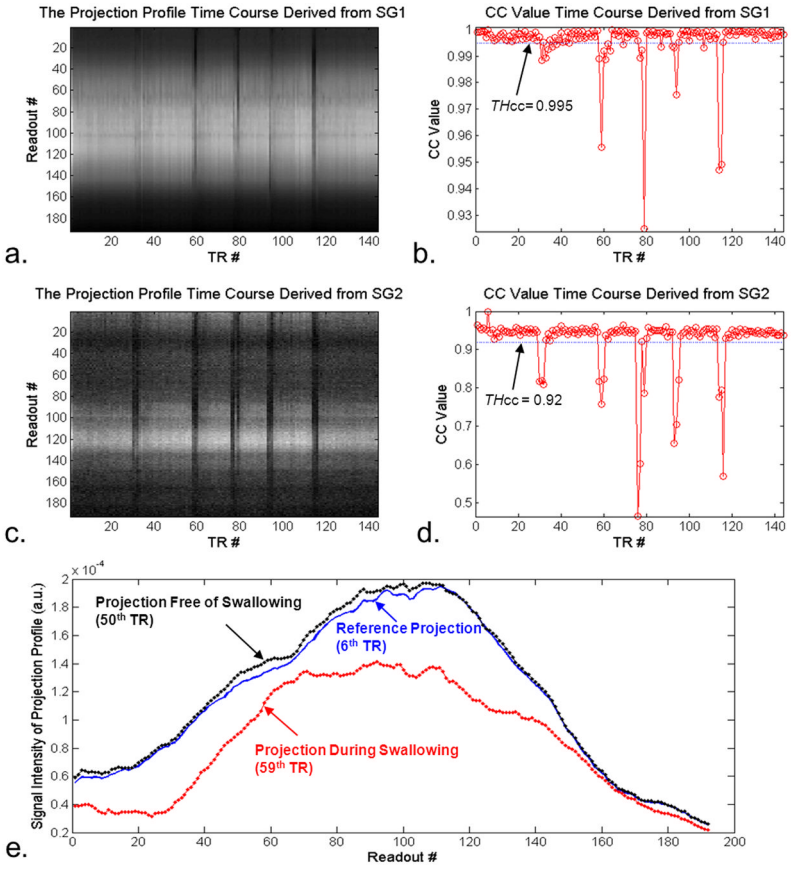


**Fig. 3.**

Processing of the SG signals from a “SPACE SWL+SG” scan in a healthy volunteer illustrates how the SG method detects swallowing motion. The time courses of projection profiles (a. and c.) and cross-correlation coefficients (CC) (b. and d.) obtained from $SG_1$ and $SG_2$, respectively, clearly demonstrates that instructed swallowing events are always detected by either or both of the two SG signals. In contrast to the projection profiles devoid of motion, motion-contaminated projection profiles deviate substantially in shape and magnitude from the reference projection profile (e.).

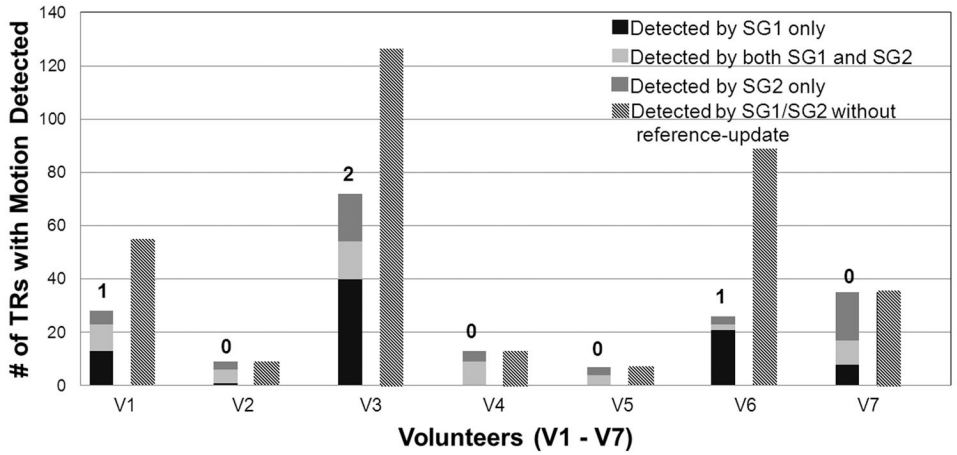


**Fig. 4.**

Retrospective analysis of SG signals from the "SPACE SWL+SG" scans in all eight human subjects (V1 – V7) determines the number of TRs that have motion present. The left and right bars of each subject represent those numbers when the real-time "SG-reference update" was performed and not performed (using the SG line from the 6$^{th}$ TR only as the reference profile), respectively. The real-time "SG-reference update" occurred once or twice in subjects #1, #3, and #6, as indicated by the numbers above the left bars. Omission of this procedure would give rise to a drastic increase in scan times, presumably because the data acquisition could be stalled with an "outdated" reference profile. With the "SG-reference update" activated, the numbers of TRs with motion detected respectively by $SG_1$ and $SG_2$ were calculated, as shown in the stacked left bars. In all subjects, swallowing motion was not always detected simultaneously by both $SG_1$ and $SG_2$, suggesting the necessity of the dual-gate procedure.

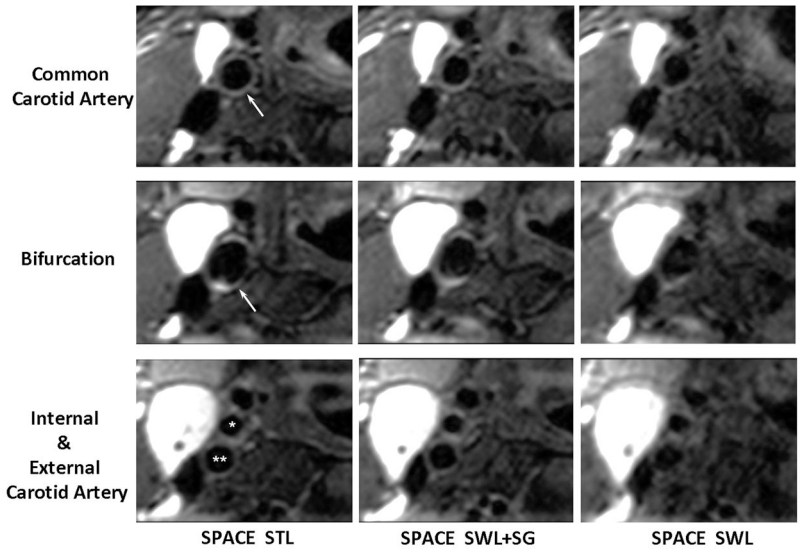


**Fig. 5.**

Comparison of location-matched transversal images obtained from the “SPACE STL”, “SPACE SWL+SG”, and “SPACE SWL” scans, respectively, in an 18-year-old female volunteer. Shown are three 2-mm-thick MPR images located below, at, and above the carotid bifurcation (arrows and star symbols), which are reconstructed from the 3D image sets. Swallowing was shown to induce severe overall image degradation, obscure wall boundary, and reduce the wall-to-background contrast. The proposed SG approach significantly mitigated the above problems and provided good artery wall delineation and high wall-to-background contrast, which is comparable to “SPACE STL” imaging. All images are displayed with the same window level. *, external carotid lumen; **, internal carotid lumen.

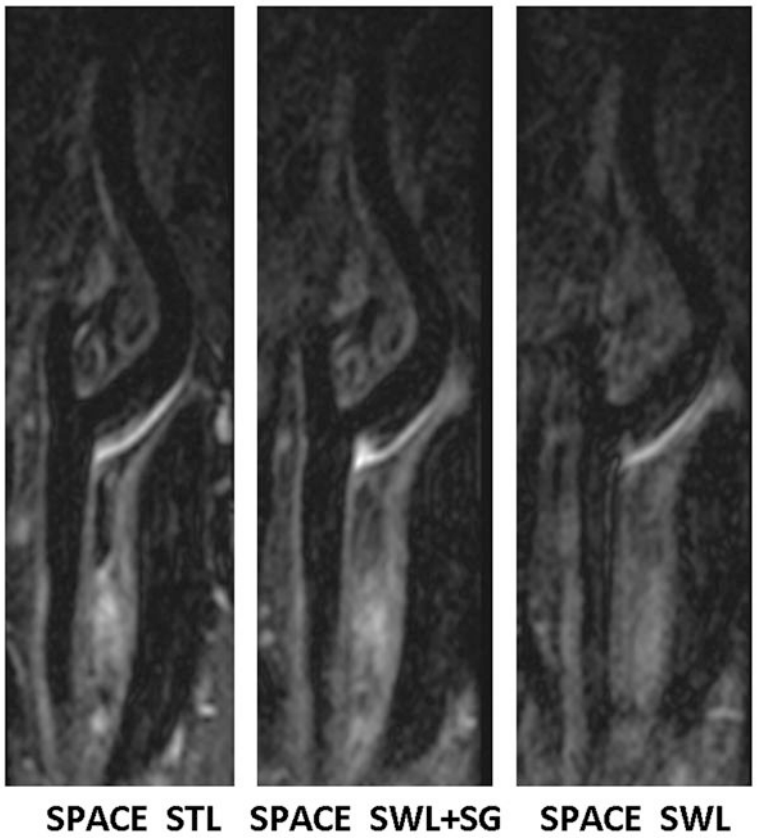


**Fig. 6.**

Comparison of location-matched longitudinal MPR images obtained from the “SPACE STL”, “SPACE SWL+SG”, and “SPACE SWL” scans, respectively, in a 45-year-old male volunteer. Shown are three 2-mm-thick images reconstructed from the 3D image sets. Swallowing was shown to induce severe overall image degradation, obscure wall boundary, and reduce the wall-to-background contrast. The proposed SG approach makes SPACE immune to swallowing motion, providing good artery wall delineation and high wall-to-background contrast that is comparable to “SPACE STL” imaging. All images are displayed with the same window level.

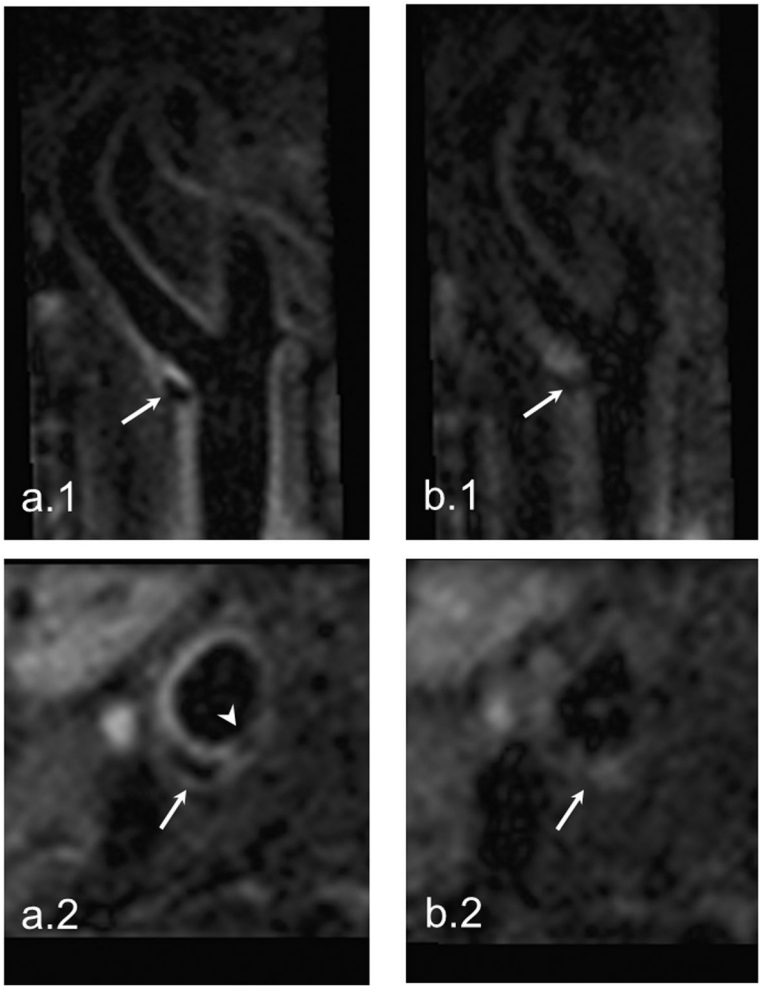


**Fig. 7.**

The SG-SPACE images (a.1 and a.2) of a 75-year-old patient with a history of transient ischemic attack and random occurrences of shortness of breath demonstrate an atherosclerotic plaque at the bifurcation of right carotid artery (arrows). The calcification and thin fibrous cap in the shoulder region (arrowhead) that are important characters of vulnerable plaques are clearly depicted. However, severe motion artifacts in regular SPACE imaging result in non-diagnostic image quality (b.1 and b.2).

**Table 1**

Image quality scores (5-point scale: 0, nondiagnostic - 4, excellent. Evaluated by two reviewers. Half-point scores allowed.) obtained in the “SPACE STL”, “SPACE SWL+SG”, and “SPACE SWL” scans. The scores obtained from the “SPACE SWL+SG” scan were compared with those obtained from two other scans.

| Subject | SPACE STL | | SPACE SWL+SG | | SPACE SWL | |
|---|---|---|---|---|---|---|
| | Left | Right | Left | Right | Left | Right |
| #1 | 3 | 3 | 2 | 2.5 | 1.5 | 1.5 |
| #2 | 4 | 4 | 3.5 | 3.5 | 1.5 | 1.5 |
| #3 | 2 | 2 | 1 | 1.5 | 1 | 1 |
| #4 | 3 | 3 | 3 | 3 | 1.5 | 2 |
| #5 | 3.5 | 3.5 | 2.5 | 2.5 | 0.5 | 0.5 |
| #6 | 3.5 | 3.5 | 2 | 2 | 0.5 | 1 |
| #7 | 3 | 3.5 | 2 | 2 | 0.5 | 0.5 |
| Mean ± Standard Deviation | 3.2 ± 0.6 | | 2.4 ± 0.7 | | 1.1 ± 0.5 | |
| *p*-value[†] | 0.002 | | N/A | | 0.001 | |

[†]Paired Wilcoxon signed rank test (n = 14, one sample per carotid)